

Effect of external magnetic field on resistance spot welding of aluminium to steel

Shanqing Hu, Amberlee S. Haselhuhn, Yunwu Ma, Zhuoran Li, Lin Qi, Yongbing Li, Blair E. Carlson & Zhongqin Lin

To cite this article: Shanqing Hu, Amberlee S. Haselhuhn, Yunwu Ma, Zhuoran Li, Lin Qi, Yongbing Li, Blair E. Carlson & Zhongqin Lin (2022) Effect of external magnetic field on resistance spot welding of aluminium to steel, Science and Technology of Welding and Joining, 27:2, 84-91, DOI: [10.1080/13621718.2021.2013707](https://doi.org/10.1080/13621718.2021.2013707)

To link to this article: <https://doi.org/10.1080/13621718.2021.2013707>



Published online: 10 Dec 2021.



Submit your article to this journal [↗](#)



Article views: 262



View related articles [↗](#)



View Crossmark data [↗](#)

RESEARCH ARTICLE



Effect of external magnetic field on resistance spot welding of aluminium to steel

Shanqing Hu^{a,b}, Amberlee S. Haselhuhn^c, Yunwu Ma^a, Zhuoran Li^{a,b}, Lin Qi^{a,b}, Yongbing Li^{a,b}, Blair E. Carlson^c and Zhongqin Lin^{a,b}

^aShanghai Key Laboratory of Digital Manufacture for Thin-walled Structures, School of Mechanical Engineering, Shanghai Jiao Tong University, Shanghai, People's Republic of China; ^bState Key Laboratory of Mechanical System and Vibration, School of Mechanical Engineering, Shanghai Jiao Tong University, Shanghai, People's Republic of China; ^cManufacturing Systems Research Lab, General Motors Global R&D, Warren, MI, USA

ABSTRACT

Resistance spot welding of aluminium to steel with magnetic-assisted apparatus was performed for the first time to understand the metallurgical joining mechanism in the melt region and at the material interface. The electromagnetic force promoted circular motion of the molten metal and accelerated the diffusion of Fe atoms to the aluminium sheet, which induced finer grains, thinner intermetallic compound layers, reduced interface defects, and elevated hardness of the resulting aluminium nugget. Coach peel tests revealed that welds made with an external magnetic field presented enhanced strength and ductility compared to welds made with no external magnetic field. The enhanced strength and ductility resulted in a transition of the fracture behaviour from brittle interfacial mode to ductile button pullout mode, and increased the peak load and the energy absorption by 90% and 1327%, respectively.

ARTICLE HISTORY

Received 8 June 2021
Revised 25 October 2021
Accepted 28 October 2021

KEYWORDS

Resistance spot welding; dissimilar materials; external magnetic field; oxide film defects; intermetallic compound

Introduction



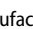
The mixed-use of dissimilar materials has been a significant method to achieve emission reduction targets in vehicle manufacturing industry [1,2]. Resistance spot welding (RSW) of dissimilar materials such as aluminium (Al) and steel offers a cost-effective way to manufacture hybrid structures. However, the direct joining of aluminium to steel by a traditional RSW process is challenging due to the thick brittle intermetallic compound (IMC) that forms at the faying interface and can significantly worsen weld mechanical behaviour [3]. In addition, oxide film defects present in the aluminium at the faying interface act as low-energy crack paths under an external applied load in dissimilar Al-steel RSW [4,5], which also degrades the mechanical performance of welds.

Some improved RSW processes, such as introducing a metallic interlayer between the aluminium and steel sheet [6] and using Multi-Ring Domed (MRD) electrode [7] were proposed to reduce the IMC thickness and break the oxide film at electrode-aluminium surface to obtain quality welds. However, the mentioned methods still possess limitations since aluminium oxide film defects could not fully be resolved,

particularly in magnesium-rich aluminium alloys such as AA5754 [4,5].

Magnetic assisted RSW has been proposed for the RSW of similar metals, e.g. like-to-like welds comprised of steels [8–10], aluminium alloys [11], or magnesium alloys [12]. The flow of molten metal in the nugget was enhanced by Lorentz force which decreased the temperature gradient in the molten nugget and prevented solidification-induced defects. The intense stirring also increased nugget size, refined grains, and improved weld mechanical performance [13,14]. However, analogous work on EMF-assisted RSW of dissimilar welds comprised of aluminium and steel is not present in the literature. The influence of electromagnetic force (EMF) on the microstructural evolution and element diffusion at the dissimilar material interface is also unknown.

To address these fundamental questions, the current study introduced EMF in the RSW of aluminium to steel with the goal to introduce the motion of molten metal to eliminate pores and the oxide film defects at the faying surface. The effects of EMF on the nugget formation, IMC growth, interfacial element diffusion, and the improvement of weld mechanical properties were also evaluated.

CONTACT Yongbing Li  yongbinglee@sjtu.edu.cn  Shanghai Key Laboratory of Digital Manufacture for Thin-walled Structures, School of Mechanical Engineering, Shanghai Jiao Tong University, Shanghai 200240, People's Republic of China  State Key Laboratory of Mechanical System and Vibration, School of Mechanical Engineering, Shanghai Jiao Tong University, Shanghai 200240, People's Republic of China

Experimental procedures

Materials, welding schedule and welding equipment

About 1.2 mm thick aluminium alloy AA5754-O and 2.0 mm thick hot-dipped galvanised low carbon steel (HDG LCS) sheets with the dimension of 127×38 mm were used in the study. The RSW process was performed on a MF-DC servo welder with water-cooled ball-nosed electrodes having a 19 mm body diameter and a 25 mm radius curved surface. The welding schedule had a preheat current of 7 kA for 40 ms and a constant current of 10 kA for 400 ms. The electrode force was kept at 3.5 kN for the entire welding process. The aluminium sheet was welded in the positive polarity condition. A pair of hollow cylinder-shaped NdFeB permanent magnets were installed on the electrodes. The dimensions and properties of the magnets are provided in Table 1. The magnetic flux density measured by YHT103 series Gauss Meter along +X-direction is presented in Figure 1.

Figure 2(a) is a schematic diagram of a magnetic-assisted apparatus [15,16] in which the same magnetic poles are aligned in opposition to one another. Figure 2(b) illustrates the directions of the induced and the external magnetic fields. Under this configuration, a Lorentz force in the circumferential direction would be generated by the interaction of external magnetic field and welding current to promote circular motion of the molten metal inside the weld nuggets, refer to Figure 2(c). Under the combined action of the induced and the external magnetic fields [17,18], the

Lorentz force increased monotonically from the centre to the edge of the nugget [13], which would drive molten metal from the weld centre towards the outer perimeter.

Metallurgical and mechanical examination

The as-polished specimens were sectioned along the weld centre and were etched by Keller's reagent to visualise weld nugget boundaries. Electron backscattered diffraction (EBSD) of the nuggets and IMC layer was performed on a TESCAN MIRA3 scanning electron microscope (SEM). The element distribution of the oxide film defects and within the aluminium nugget were identified using time of flight secondary ion mass spectrometry (TOF-SIMS) on a TESCAN GAIA3 SEM. The FEI Talos F200X transmission electron microscope (TEM) and transmission Kikuchi diffraction (TKD) were conducted to identify the Fe-rich compound in magnetic-assisted RSW (MA-RSW) aluminium nugget, which was extracted by focused ion beam (FIB). Finer scale observation of fracture surfaces applied secondary electron and backscattered electron imaging on a Vega SEM with a 20 kV accelerating voltage.

Microhardness testing was conducted on a Buehler Wilson VH1102 hardness tester with 50 g load, 0.2 mm pitch and 10 s dwell time. Coach peel testing was performed to evaluate the weld mechanical properties on a SUNS tensile machine by fixing the steel sheet and pulling the aluminium sheet, which was welded to the steel sheet, at a rate of 5.0 mm min^{-1} as described in

Table 1. Dimensions and properties of the NdFeB permanent magnet.

Height (mm)	Outside diameter (mm)	Inside diameter (mm)
10	24	21
Remanence magnetic induction (B_r/T) 1.41	Intrinsic coercive magnetic field ($H_{ci}/\text{kA m}^{-1}$) 1158	Maximum magnetic energy $((BH)_{\max}/\text{kJ m}^{-3})$ 493

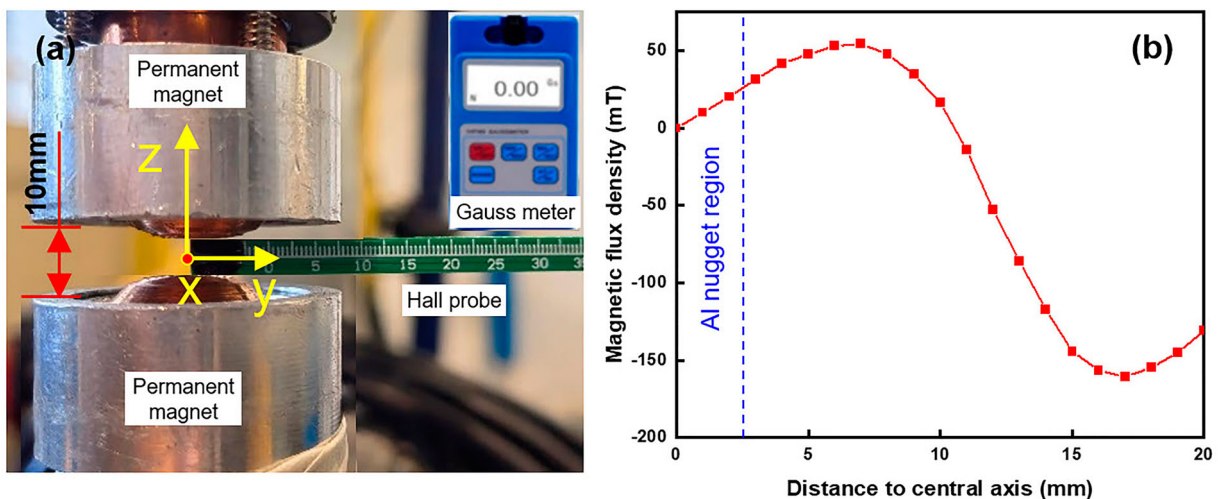


Figure 1. Measurement of the radial magnetic flux density. (a) Measurement position and setup. (b) Intensity of the radial magnetic flux density on the faying surface of workpieces.

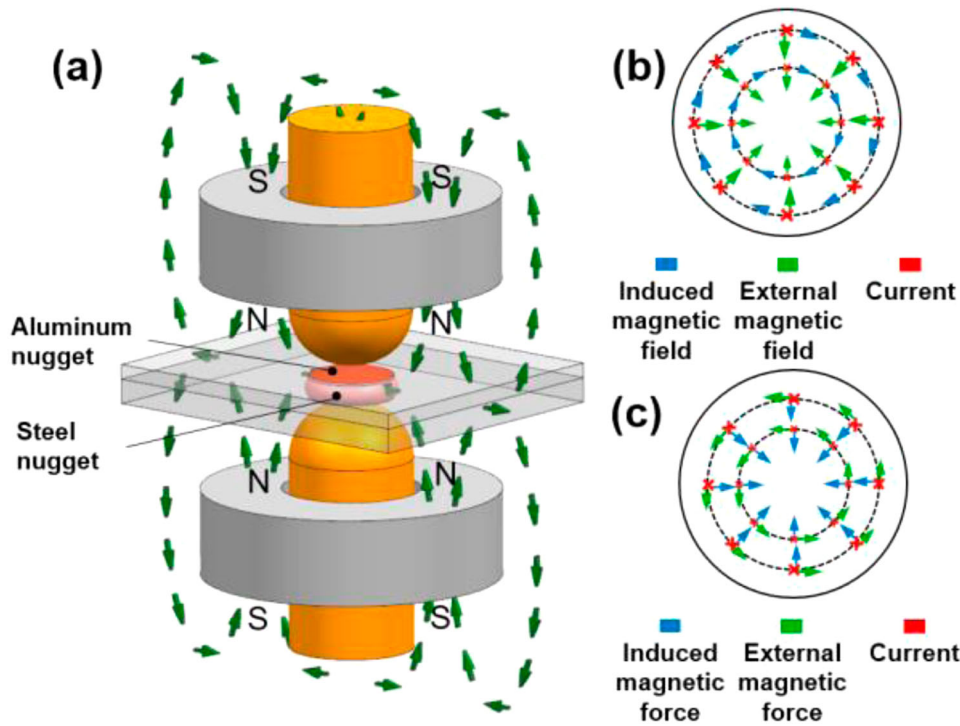


Figure 2. Sketch of magnetic field distribution in weld nugget. (a) RSW process with magnetic-assisted apparatus. (b) Magnetic field distribution at the faying surface. (c) Magnetic force at the faying surface.

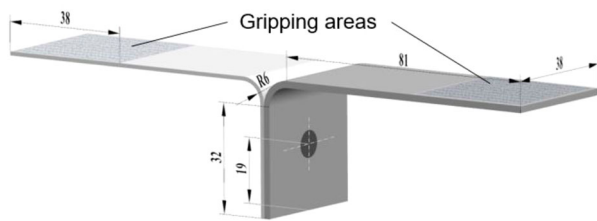


Figure 3. Schematic diagram of spot weld locations on coach peel coupon. All units are in mm.

previous work [4]. The coach peel specimens were presented in Figure 3.

Results and discussion

Weld morphology and grain size

Referring to Figure 4(a,b), it can be observed that the joint structure exhibits two nuggets, one in the aluminium sheet and one in the steel sheet. The nugget in the aluminium sheet initiated from and directionally solidified against the steel sheet. No melting and subsequent mixing of the steel sheet with the aluminium sheet occurred at the faying interface. Thus, any electromagnetic force occurred within each of the separate nuggets. The MA-RSW joint exhibited a smaller aluminium nugget with a 5.1 mm diameter but a larger steel nugget with a 7.2 mm nugget diameter compared to the RSW joint, whose aluminium and steel nuggets diameter were 5.5 and 7.0 mm respectively. According to Shen et al. [10], the external magnetic field can enhance the heat transfer from the centre to the edge

of the molten pool when used to join similar metals. As a result, the temperature history and thermal gradient in the nugget diameter direction were decreased and a larger nugget diameter was achieved. Similarly, the MA-RSW joint of Al-steel produced a larger steel nugget than the RSW joint did in this study. In traditional Al-steel RSW, 75% of the heat generation occurs in the steel sheet [19] and conduction aids in heating the aluminium sheet, which grows the weld nugget in the aluminium sheet. In the MA-RSW process, because of greater heat transfer from nugget centre to edge in the steel sheet, there is less heat transfer into the aluminium sheet resulting in reduced penetration and weld nugget diameter of the aluminium weld. Moreover, the aluminium nugget in RSW weld had the sharper edge angle, which was 24.3° , compared to the characteristic in MA-RSW welds, which was 31.2° . The EMF at the nugget edge flushed the aluminium resulting in an aluminium nugget with a larger edge angle formed in MA-RSW welds.

Coarse columnar crystals were formed in both RSW and MA-RSW aluminium nuggets parallel to the penetration direction, refer to Figure 4(c,d), which is coincident with large thermal gradients between the water-cooled electrode and the high-temperature steel sheet. $31.50\ \mu\text{m}$ is the average grain width in region 1 of the MA-RSW aluminium nugget, and is 25.42% smaller than the average grain width in the RSW aluminium nugget. The average grain length was 297.57 and $345.79\ \mu\text{m}$ in MA-RSW and RSW welds, respectively. This difference is attributed to the reduced heat transfer into the aluminium sheet for the MA-RSW as

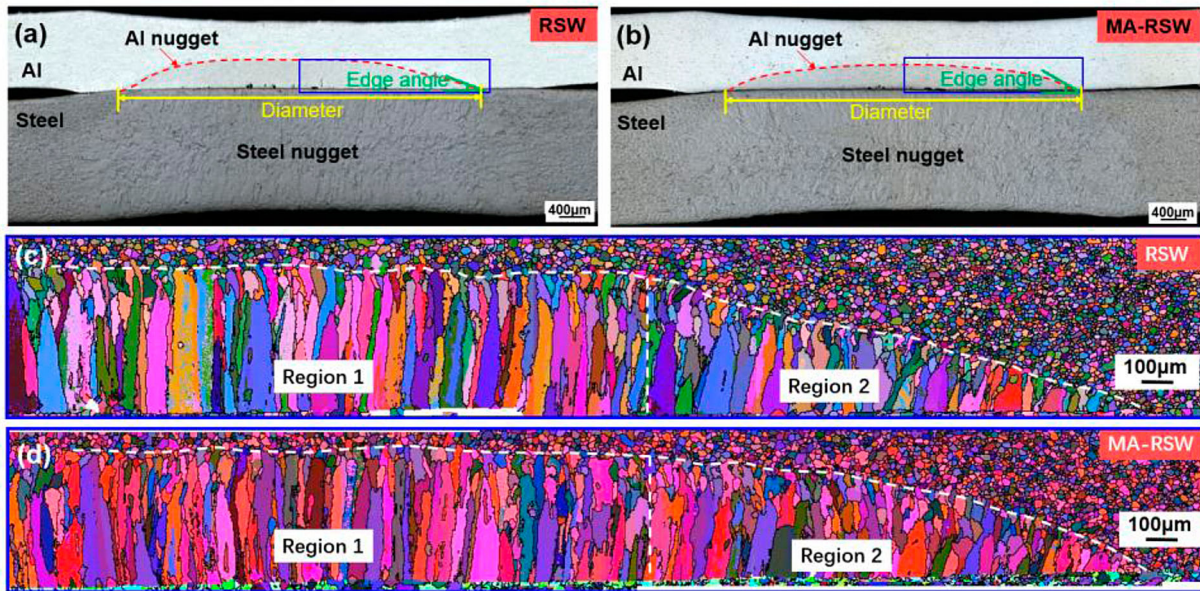


Figure 4. Macro profiles of (a) RSW and (b) MA-RSW welds. (c) EBSD images of grain distribution at the Al nugget of RSW weld in (a). (d) EBSD images of grain distribution at the Al nugget of MA-RSW weld in (b).

described above. Another unique aspect of the MA-RSW weld is the presence of a multi-layered columnar crystal structure at the edge of the nugget, i.e. region 2, where the electromagnetic force was the strongest. This structure formed because the Lorentz force induced flow broke the growth of columnar dendrites and solidification occurring from broken columnar tips resulting in grain refinement at the nugget edge. This multi-layered structure has been demonstrated to improve the ability of MA-RSW to resist crack propagation compared to traditional RSW [20].

Weld defects

Weld mechanical properties are sensitive to IMC layer thickness and defects at the faying surface [21]. Pore defects were observed in both RSW and MA-RSW nuggets along the IMC/Al weld nugget interface. As can be observed in Figure 5(a,b), the size of the pores as measured from the interface into the weld nugget is comparable however, the cross-section area of the pore defects in MA-RSW and RSW nugget was 0.48 and 17.99 mm², respectively, which supports the concept of EMF in the MA-RSW weld pool breaking up the defects.

Amounts of linear defects floating at the faying surface in the RSW aluminium nugget were observed as

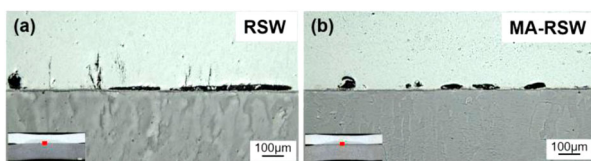


Figure 5. Pore defects at the centre of faying surface. (a) RSW and (b) MA-RSW.

well, refer to Figure 6(a). These defects were further identified using TOF-SIMS and the elements distribution were shown in Figure 6(b–d). Their presence is attributed to the aggregation of O, Mg and Al, which should be oxide film inclusions [5,22]. The non-melt oxide film inclusions defects, from the natural oxide on the aluminium sheet, acted as low-energy cracks path to degrade weld mechanical properties in both the as-welded and baked condition upon application of an external load [4,5].

IMC characteristics

The steel and aluminium sheets were bonded by a layer of IMCs at the faying interface, which with increasing thickness, increases crack susceptibility and reduces weld ductility [3]. The IMC compositions and morphologies of RSW and MA-RSW welds were further identified using EBSD, which are presented in Figure 7(a,b). Both the RSW and MA-RSW IMC layers exhibited stratification wherein the thin layer close to the aluminium sheet was FeAl₃ and the dominated thick layer adjacent to the steel sheet was Fe₂Al₅. The respective thicknesses of the Fe₂Al₅ and FeAl₃ layers in the RSW weld were 9.14 and 0.64 µm, respectively. In contrast, the RSW weld exhibited a thinner Fe₂Al₅, 6.59 µm, and a slightly thicker FeAl₃ layer, 0.72 µm. According to Sun et al. [23], during the reaction of molten aluminium with steel, the Fe₂Al₅ nucleated and grew at the faying surface as the Fe atoms accumulated in liquid aluminium alloy. In the MA-RSW process, the EMF accelerated Fe atoms diffusion into the molten zone, which disturbed the nucleation of Fe₂Al₅ resulting in thinner IMC layer. The lower temperature at the faying surface in MA-RSW weld is another potential source for reducing the rate of growth of Fe₂Al₅

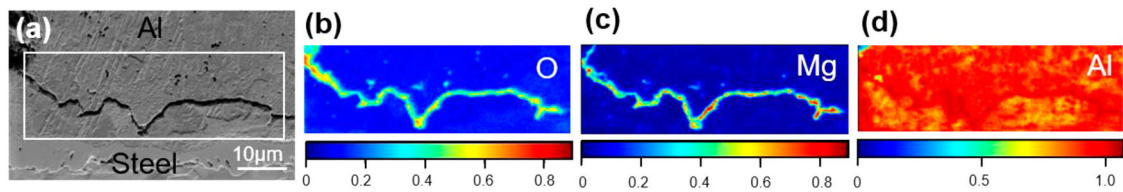


Figure 6. Oxide film defects in RSW weld. (a) Macro morphology of oxide film defects. (b–d) Relative distributions of O, Mg and Al obtained by TOF-SIMS.

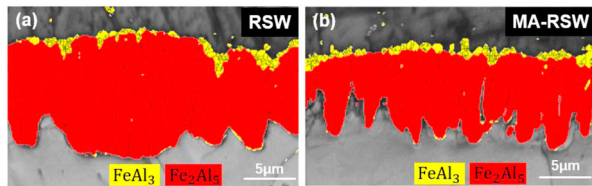


Figure 7. EBSD images of IMC phase distribution. (a) RSW and (b) MA-RSW.

since temperature directly affects diffusion and thereby determines the IMC layer thickness [24,25].

Figure 8 summarises the distribution of IMC thickness and presence of defects across the entire weld nugget where different colours represent the percentage of oxide film in the field of view and circles indicate the presence of porosity. The characteristics in evenly 11 distributed regions were observed using the optical microscope. The average IMC thickness was calculated as the area enclosed by the Al/IMC and IMC/steel boundary lines over the width of the region which was fixed at 250 µm [4]. The peak IMC thickness located near the weld nugget centreline decreased from approximately 10 µm for traditional RSW to approximately 7 µm in the MA-RSW joint. The traditional RSW process retained more oxide film defects and pores at the faying interface than MA-RSW welds. Among the 9 positions in the RSW joint, 7 of them had defects over 100% of the field of view and 6 of them exhibited pore defects. In contrast, the majority of the MA-RSW joint was defect-free, particularly of oxide film inclusion defects. EMF in the molten aluminium nugget reduced

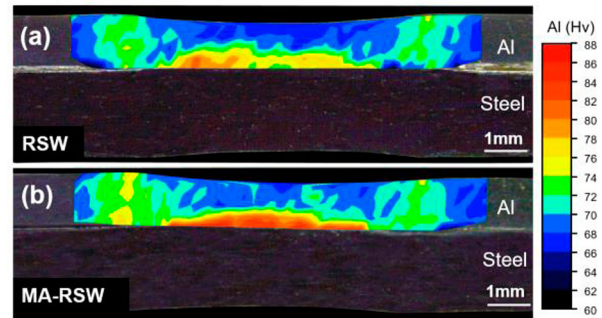


Figure 9. Hardness mapping of aluminium nuggets. (a) RSW and (b) MA-RSW.

the temperature gradient and cooling rate during solidification. This produced fewer solidification pores and prevented the coalescence of hydrogen porosity leading to fewer porosity-defects at the faying surface. Electromagnetic force in the aluminium nugget also broke apart and drove oxide film inclusions away from the faying surface. Thus, the MA-RSW weld with less defects and thinner IMC layers was expected to show better performance.

Aluminium hardness and strengthening phase

Microhardness mapping of the aluminium weld structures was conducted to evaluate the differences between RSW and MA-RSW welds, refer to Figure 9(a,b). Both RSW and MA-RSW weld nuggets were hardened compared to the base metals, though more so for the MA-RSW compared to the RSW nugget (78 HV vs. 88 HV, respectively).

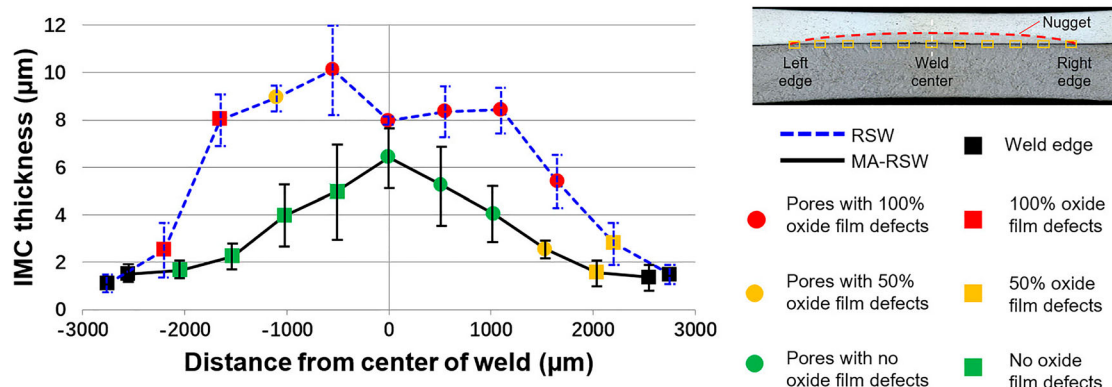


Figure 8. IMC thickness and defects distribution statistics for RSW and MA-RSW welds. Error bars represent ± 1 standard deviation.

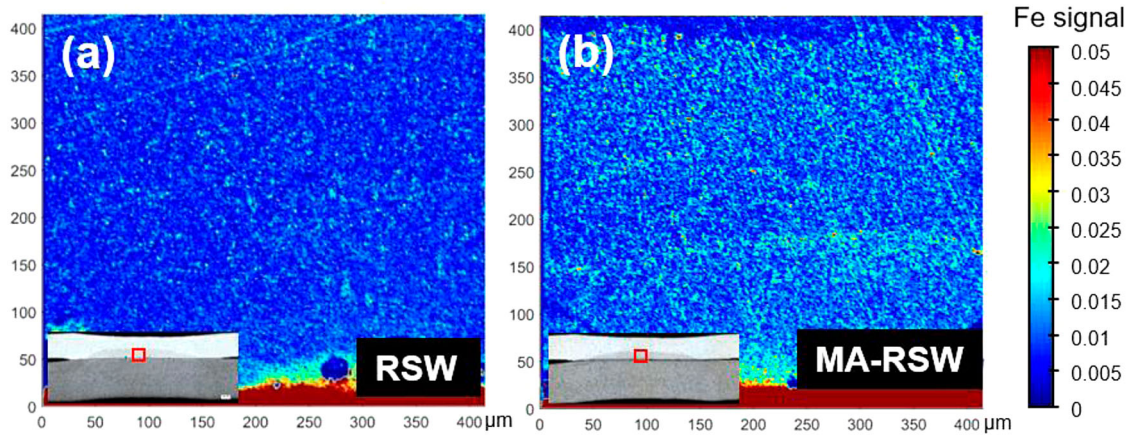


Figure 10. TOF-SIMS image of Fe distribution in the nugget area. (a) RSW and (b) MA-RSW.

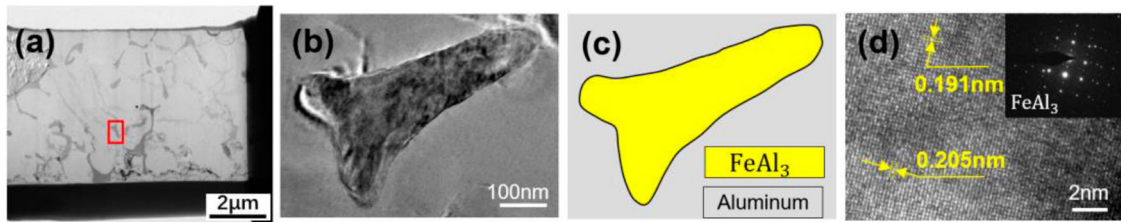


Figure 11. Precipitated phase analysis. (a) MA-RSW aluminium nugget FIB slice. (b) Bright-field image of precipitated phase. (c) TKD phases identified results. (d) High Resolution TEM image and diffraction pattern of precipitated phase.

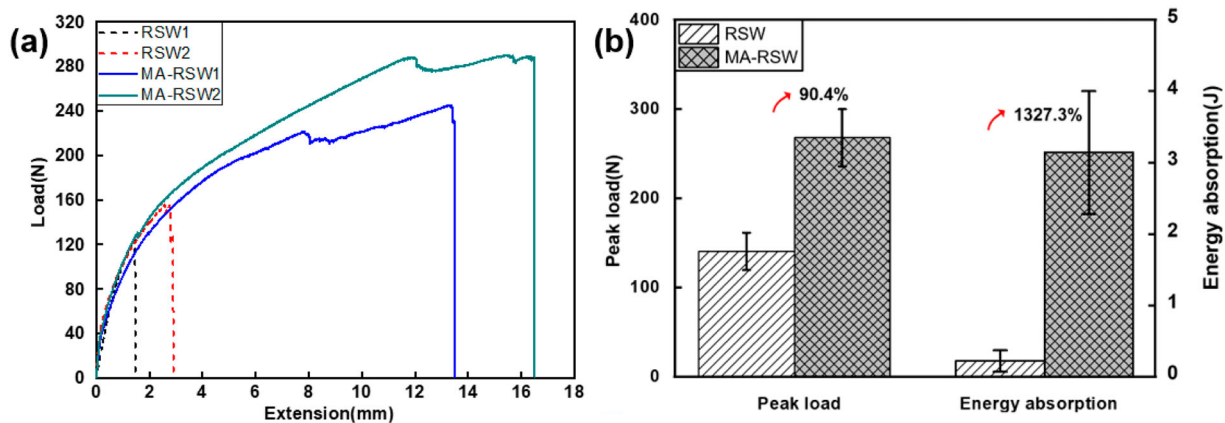


Figure 12. Coach peel performance of RSW and MA-RSW welds. (a) Load-extension curves. (b) Bar graphs of average peak load and energy absorption. Error bars represent ± 1 standard deviation.

TOF-SIMS was used to identify the difference in Fe content in the two nuggets. As presented in Figure 10(a,b), more iron diffused into the fusion zone of MA-RSW welds forming a Fe-rich precipitated phase with the assistance of EMF which contributed to the increased hardness in the aluminium structure.

To further identify Fe-rich precipitated phase, the nanoscale characterisation of the precipitated phase in MA-RSW aluminium nugget were performed using TEM and TKD, refer to Figure 11(a–d). As identified by the diffraction pattern, the precipitated phase should be FeAl_3 . The presence of FeAl_3 particles increased slip resistance, favouring the improvement of aluminium nugget strength.

Coach peel performance

Figure 12(a) presents the coach peel load-extension curves of the RSW and MA-RSW welds where a greater peak load and extension can be observed for the MA-RSW welds. The average peak load for MA-RSW welds was 268 ± 32 N, 90% greater than welds produced by traditional RSW. The average energy absorption of MA-RSW welds was 3.1 ± 0.9 J, 1327% greater compared to the RSWs, refer to Figure 12(b).

Back-scattered electron images of RSW and MA-RSW weld fracture surfaces on the steel sheets are presented in Figure 13(b,e). It should be noted that the steel substrate outside of the weld is a lighter grey colour which indicates heavy elements i.e. iron phases. The centre of the weld fracture surfaces is darker in colour

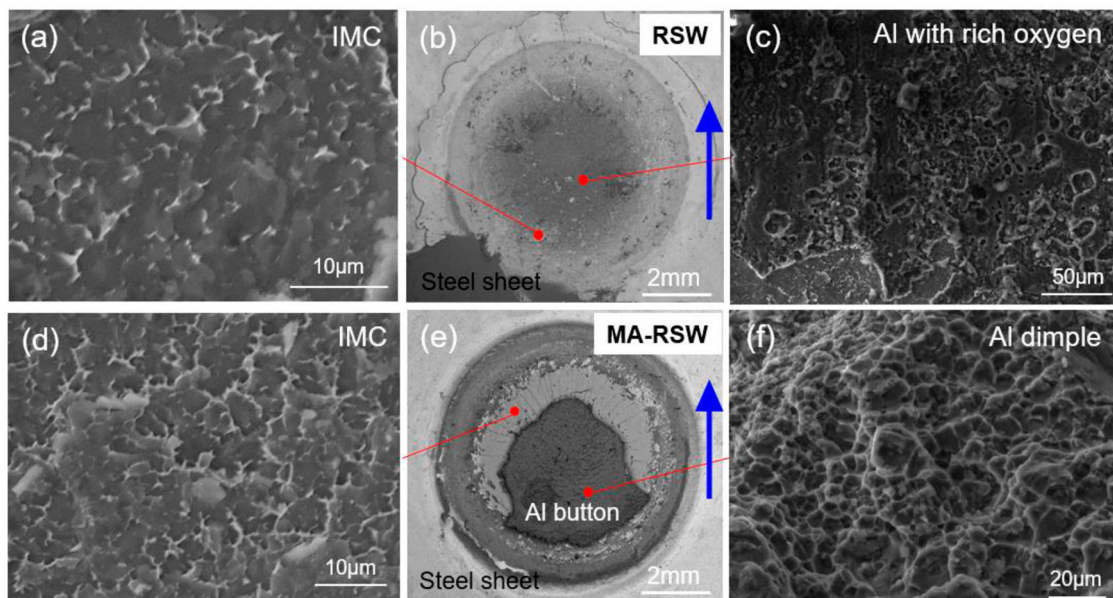


Figure 13. Fractographies of (b) RSW and (e) MA-RSW welds in back-scattered electron mode. (a, c) Partial enlarged images of the RSW weld. (d, f) Partial enlarged images of the MA-RSW weld. Blue arrow represents the direction of peel in mechanical experiments.

which indicates the surface being rich with light elements i.e. presence of aluminium. Interfacial and partial button fracture modes were observed for the RSW and the MA-RSW joins, respectively. The crack paths of RSW and MA-RSW also differed according to the SEM images. The fracture surface of the RSW weld exhibits a large area of dark grey indicative of brittle fracture in an oxygen-rich aluminium phase, refer to Figure 13(c). The sparse light grey areas distributed among the oxide film defect fracture surfaces correspond to the cleavage plane which was IMC, refer to Figure 13(a). Thus, cracks in the RSW primarily propagated along oxide film defects near the faying surface resulting in brittle interfacial fracture which reduced the weld mechanical properties significantly. The MA-RSW weld fracture surface contains a residual portion of aluminium on the steel sheet surrounded by a light area (IMC), refer to Figure 13(d). This aluminium exhibits many dimples, refer to Figure 13(f), indicative of a more ductile fracture. Thus, crack propagation in MA-RSW occurred partially within the aluminium nugget which was hardened by elevated iron content and partially within the IMC until complete fracture occurred, resulting in greater energy absorption as is consistent with a ductile fracture mode i.e. in this case a partial button fracture mode.

Conclusions

This body of work investigated the effect of external magnetic field on dissimilar resistance spot welds of 5754-low carbon steel. The weld morphology, grain size, microstructural defects, IMC characteristics, weld hardness and coach peel performance of the RSW and

MA-RSW welds were systematically compared. The following conclusions are derived from this work:

- The external magnetic field induced EMF within aluminium nugget resulting in a smaller unique aluminium nugget microstructure with refined grain size, a multi-layer structure at the edge regions, and a larger edge angle.
- The EMF in aluminium nugget drove the oxide film away from the interface and inhibited the aggregation of oxide film and pores defects at the faying surface.
- The EMF in aluminium nugget also accelerated the Fe atoms diffusion into aluminium nugget which disturbed the IMC nucleation and decreased the peak IMC thickness by 30%. The more Fe atoms in aluminium nugget formed more precipitated phase (FeAl_3) which increased aluminium nugget hardness from 78HV to 88HV.
- All of these factors improve the ability to resist crack propagation when the external load is applied and lend themselves to the development of a strong aluminium nugget with ductile fracture mode. The peak load and energy absorption of coach peel samples improved 90% and 1327%, respectively with the assist of the external magnetic field.

Acknowledgements

The authors thank Chad Clark (Fusion Welding Solutions) for his welding expertise and valuable discussions.

Disclosure statement

No potential conflict of interest was reported by the author(s).

Funding

This work was supported by National Natural Science Foundation of China [Grant Number 52025058]; National Natural Science Foundation of China [Grant Number U1764251]; State Key Laboratory of Mechanical System and Vibration [Grant Number MSVZD202111].

References

- [1] Tanaka T, Morishige T, Hirata T. Comprehensive analysis of joint strength for dissimilar friction stir welds of mild steel to aluminum alloys. *Scripta Mater.* 2009;61:756–759.
- [2] Rest C, Jacques PJ, Simar A. On the joining of steel and aluminium by means of a new friction melt bonding process. *Scripta Mater.* 2014;77:25–28.
- [3] Martinsen K, Hu SJ, Carlson BE. Joining of dissimilar materials. *CIRP Ann.* 2015;64:679–699.
- [4] Hu SQ, Haselhuhn AS, Ma YW, et al. Comparison on resistance spot weldability of AA5754/steel and 6022/steel. *Weld J.* 2020;99:224s–238s.
- [5] Hu SQ, Haselhuhn AS, Ma YW, et al. Influencing mechanism of inherent aluminum oxide film on coach peel performance of baked Al-steel RSW. *Mater Design.* 2021;197:109250.
- [6] Oikawa H, Ohmiya S, Yoshimura T, et al. Resistance spot welding of steel and aluminium sheet using insert metal sheet. *Sci Technol Weld Join.* 1999;4:80–88.
- [7] Sigler DR, Schroth JG, Karagoulis MJ, et al. New electrode weld face geometries for spot welding aluminum. *Sheet Metal Welding Conference XIV.* 2010.
- [8] Li YB, Zhang QX, Qi L, et al. Improving austenitic stainless steel resistance spot weld quality using external magnetic field. *Sci Technol Weld Join.* 2018;23:619–627.
- [9] Qi L, Li FZ, Chen RM, et al. Improve resistance spot weld quality of advanced high strength steels using bilateral external magnetic field. *J Manuf Process.* 2020;52:270–280.
- [10] Shen Q, Li YB, Lin ZQ, et al. Effect of external constant magnetic field on weld nugget of resistance spot welded dual-phase steel DP590. *IEEE T Magn.* 2011;47:4116–4119.
- [11] Yao Q, Luo Z, Li Y, et al. Effect of electromagnetic stirring on the microstructures and mechanical properties of magnesium alloy resistance spot weld. *Mater Design.* 2014;63:200–207.
- [12] Huang M, Zhang QX, Qi L, et al. Effect of external magnetic field on resistance spot welding of aluminum alloy AA6061-T6. *J Manuf Process.* 2020;50:456–466.
- [13] Li YB, Li DL, David SA, et al. Microstructures of magnetically assisted dual-phase steel resistance spot welds. *Sci Technol Weld Join.* 2016;21:555–563.
- [14] Qi L, Li FZ, Zhang QX, et al. Improvement of single-sided resistance spot welding of austenitic stainless steel using radial magnetic field. *J Manuf Sci E.* 2021;143:1–11.
- [15] Li YB, Lin ZQ, Li RH, et al. Magnet resistance spot welding system. 2011, CN101628358A.
- [16] Li YB, Qi L, Lou M. Split magnets resistance spot welding device. 2020, CN108788419B.
- [17] Li YB, Lin ZQ, Hu SJ, et al. Magneto hydrodynamic behaviors in a resistance spot weld nugget under different welding currents. *Sci China Ser E Technol Sci.* 2008;51:1507–1515.
- [18] Li YB, Lin ZQ, Lai XM, et al. Induced electromagnetic stirring behavior in a resistance spot weld nugget. *Sci China Technol Sci.* 2010;53:1271–1277.
- [19] Wan ZX, Wang HP, Wang M, et al. Numerical simulation of resistance spot welding of Al to zinc-coated steel with improved representation of contact interactions. *Int J Heat Mass Tran.* 2016;101:749–763.
- [20] Li Y, Luo Z, Yan FY, et al. Effect of external magnetic field on resistance spot welds of aluminum alloy. *Mater Design.* 2014;56:1025–1033.
- [21] Chen NN, Wang HP, Carlson BE, et al. Fracture mechanisms of Al/steel resistance spot welds in coach peel and cross tension testing. *J Mater Process Technol.* 2018;252:348–361.
- [22] Sigler DR, Carlson BE. Impediments to developing resistance spot welding processes for joining aluminum to steel. *Conference proceedings AWS Sheet Metal Welding Conference XVIII.* 2018.
- [23] Sun DQ, Zhang YY, Liu YJ, et al. Microstructures and mechanical properties of resistance spot welded joints of 16Mn steel and 6063-T6 aluminum alloy with different electrodes. *Mater Design.* 2016;109:596–608.
- [24] Bouayad A, Gerometta C, Belkebir A, et al. Kinetic interactions between solid iron and molten aluminium. *Mat Sci Eng A.* 2003;363:53–61.
- [25] Springer H, Kostka A, Payton EJ, et al. On the formation and growth of intermetallic phases during interdiffusion between low-carbon steel and aluminum alloys. *Acta Mater.* 2011;59:1586–1600.